

Electronic structure and energetics of sapphire (0001) and ($\bar{1}\bar{1}02$) surfaces

J. Guo, D. E. Ellis, and D. J. Lam

Materials Science Division, Argonne National Laboratory, Argonne, Illinois 60439

(Received 8 October 1991; revised manuscript received 17 December 1991)

Electronic structure and energetics of (0001) and ($\bar{1}\bar{1}02$) surfaces of sapphire, α -Al₂O₃, were calculated using the self-consistent-field discrete variational (DV) method in the local-density framework. Clusters of a size of 70–120 atoms embedded in the semi-infinite host lattice were used to model the sapphire free surfaces. Calculations were performed on all possible terminating (0001) and ($\bar{1}\bar{1}02$) surfaces obtained from cleaving a sapphire single crystal. The energetic calculations show that the surface with the lowest cleavage energy is terminated with an Al layer for the (0001) surface, while it is terminated with an O layer for the ($\bar{1}\bar{1}02$) surface. The concept of the *surface building block*, useful in determining the surface atomic termination, was proposed. Two unoccupied surface bands derived from the top-layer Al atoms are found within the bulk band gap at 2 and 8 eV below the conduction-band minimum (CBM) for the (0001) surface. For the ($\bar{1}\bar{1}02$) surface, the occupied valence states derived from 2*p* states of the top-layer O atoms are found \sim 4.0 eV below the CBM, which may explain the 4.7-eV energy-loss feature found experimentally on a sapphire ($\bar{1}\bar{1}02$) surface.

I. INTRODUCTION

Various crystallographic faces of sapphire, the undoped single crystal α -Al₂O₃, have been widely used as substrates for depositing thin films of metals, semiconductors, and insulators for basic scientific studies and for microelectronic applications.¹ The lattice structure of these faces has been studied by many experimental techniques. Low-energy electron diffraction (LEED) revealed that the (0001) crystal surface exhibits a (1×1) bulk-like structure below \sim 1250 °C in air or in vacuum. Annealed in air above 1400 °C or in vacuum above \sim 1250 °C, the surface rearranges to give a ($\sqrt{3}\times\sqrt{3}$)R30° or ($\sqrt{3}\bar{1}\times\sqrt{3}\bar{1}$)R9° surface structure.^{2–6} LEED results also indicated reconstruction of the ($\bar{1}012$) and (11 $\bar{2}$ 3) surfaces of α -Al₂O₃ after heating to high temperature in the LEED system.⁷ The two-dimensional lattice for the reconstructed ($\bar{1}012$) and (11 $\bar{2}$ 3) surfaces are relatively simple (2×1) and (4×5), respectively. The surface structure of the (11 $\bar{2}$ 0) face of α -Al₂O₃ has been studied by Yao, Wang, and Cowley⁸ using a combination of reflection electron microscopy (REM), reflection high-energy electron diffraction (RHEED), and reflection electron-energy-loss spectroscopy (REELS). They did not report reconstruction of the (11 $\bar{2}$ 0) surface but suggested the cleaved surfaces contained oxygen-rich and alumina-rich domains. Recent transmission electron microscopy (TEM) and LEED results indicated that the (11 $\bar{2}$ 0) surface will reconstruct after annealing at 1400 °C. However, the reconstructed lattice structure was reported by Sunitzky and Carter⁵ to be a (1×2) structure whereas Hsu and Kim⁹ suggested a (1×4) structure.

The nature of the atomic termination layers on sapphire surfaces is important to the understanding of the effects of substrate structure on the epitaxial relationship and the overlayer lattice structure of thin-film deposi-

tion. The electronic structure of sapphire ($\bar{1}\bar{1}02$) surfaces has been studied by Gignac, Williams, and Kowalczyk¹⁰ using x-ray photoelectron spectroscopy (XPS) and the electron-energy-loss-spectroscopy (EELS) method. The combined XPS and EELS results were used to construct a one-electron energy-level diagram. They found a band-gap state occurring at \sim 4 eV below the conduction-band minimum. Based on the similarity between the energy location of the band-gap state and the surface-state energy position of a sapphire (0001) surface calculated by Ciraci and Batra¹¹ using a semiempirical method, they concluded that the observed band-gap state is a surface state due to an Al-terminated ($\bar{1}\bar{1}02$) sapphire surface. Despite this inference, there is no experimental proof to indicate that Al atoms indeed form the topmost layer of either the (0001) or the ($\bar{1}\bar{1}02$) sapphire surfaces. As mentioned earlier, Yao *et al.* suggested that the (11 $\bar{2}$ 0) surface of α -Al₂O₃ can be terminated with either O-rich or Al-rich top-surface monolayers.

The first-principles local-density self-consistent-field (SCF) embedded-cluster method is a useful scheme for studying electronic structure and energetics of complex oxide systems, containing substituent ions and defects.^{12–17} Recently, improvements in the cluster calculations have resulted from advances in the embedding scheme and more ample choices of the cluster sizes and shapes.^{18,19} In our recent paper on bulk sapphire,¹⁹ we have established the size of clusters needed and the level of accuracy obtainable within the embedded-cluster model, using the self-consistent charge scheme and the concept of *seed atoms*.

In the present paper, we have used the SCF embedded-cluster method to study electronic structure and energetics of unreconstructed sapphire (0001) and ($\bar{1}\bar{1}02$) surfaces with all possible termination layers obtained from cleaving a sapphire single crystal. The second sec-

tion of the paper gives details in methodology of treating the semi-infinite surfaces in the discrete variational embedded-cluster method. The third section presents the calculated energetic results for all possible surface terminations of (0001) and $(1\bar{1}02)$ surfaces, and the electronic structure of the two surfaces with the lowest cleavage energy. The calculated electronic structure and the predicted surface states are compared with the experimental XPS and EELS results. The final section gives our conclusions.

II. THEORETICAL APPROACH

A. Crystal, surface, structures, and clusters chosen

The crystal structure of sapphire, $\alpha\text{-Al}_2\text{O}_3$, is typified by that of chromium sesquioxide, Cr_2O_3 .²⁰ It has a rhombohedral symmetry with two molecules in the primitive cell. The space group is D_{3d}^6 . The corresponding hexagonal unit cell, a larger cell containing 12 Al and 18 O atoms, is shown in Fig. 1 with $a = 4.76 \text{ \AA}$ and $c = 13.00 \text{ \AA}$.²⁰ The cell shown in Fig. 1 has the S_6 point-group symmetry with respect to its center.

1. (0001) surfaces

From Fig. 1, we see that the sapphire single crystal may be cleaved parallel to the (0001) plane at two different locations labeled *A* and *C*. Cleaving at plane *A* produces a surface terminated with an O layer and a surface terminated with two Al layers. Since the sapphire single crystal has the inversion symmetry, the (0001) and (000 $\bar{1}$) surfaces with the same termination atoms are equivalent. Cleaving at plane *C* produces two equivalent sur-

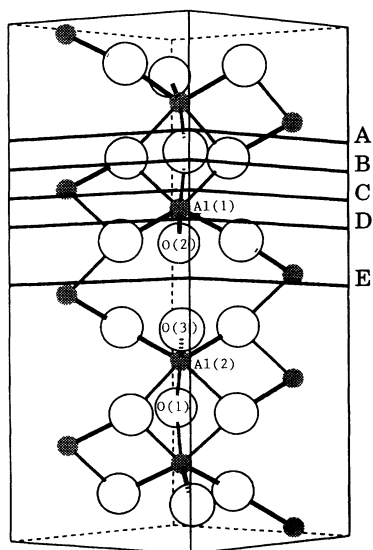


FIG. 1. A perspective view of the hexagonal unit cell of sapphire. The filled circles label Al atoms, and open circles O atoms. The dark thick lines label the short Al-O bonds (1.86 Å), the light thin lines the long Al-O bonds (1.97 Å).

faces terminated with an Al layer. Further analysis shows that any two (0001) surfaces, which have the same terminations and are cleaved at the two planes separated by $c/6 = 2.16 \text{ \AA}$ (e.g., planes *A* and *D*, planes *C* and *E*), are equivalent to one another by the mirror reflection about the $(11\bar{2}0)$ plane. Therefore, three possible (0001) surfaces with different termination layers and three corresponding symmetry-equivalent ones may be produced by cleaving the sapphire crystal perpendicular to the *c* axis. Since the total energy and other physical properties of any symmetry-equivalent surfaces are the same, we only need to study the three (0001) surfaces produced by cleaving at the planes labeled *A*, *B*, and *C* in Fig. 1.

For sapphire crystal there are only two chemically distinct atoms, i.e., Al and O. For the (0001) surfaces, the periodicity along the surface normal (*c* axis) is broken and only the two-dimensional periodicity on the surface is preserved. Therefore, the Al and O atoms at different heights from the surface become chemically distinct. Due to the two-dimensional nature of the surfaces, the cluster atoms were chosen to be within a cylinder, which contains the surface unit mesh and completely coordinated *seed* atoms. The charge density of *seed* atoms is used to construct the self-consistent surface potential. Calculations on an Al-layer-terminated surface using a larger cluster shows that the radius of 4.5 Å is large enough to achieve the desired precision in total energy and electronic structure. For the sake of comparisons, we used the radius of 4.5 Å for all three surfaces with different terminations. Calculations using clusters with larger depth show that the 8-Å depth of the cylinder down to the O atoms at the bottom of Fig. 1 is deep enough to represent the surface effects. With the axes of the cylinders passing through the center of the unit cell shown in Fig. 1, we have three clusters with C_3 symmetry and of sizes 63, 66, and 78 atoms embedded in the semi-infinite surfaces for the surfaces produced by cleaving at the planes labeled *C*, *B*, and *A* in Fig. 1, respectively. The atoms outside the cluster were treated as *host* atoms. Host atoms enter into formation of the total density and potential, but are not part of the cluster variational space. Shown in Fig. 2(a) is a top view of one surface building block made up of three atomic layers of Al-O-Al for the (0001) surface. Figure 2(b) gives a side view along the $[11\bar{2}0]$ direction of the (0001) surface, which reveals its layer structure. The other two distinct (0001) surfaces can be constructed by removing the topmost Al layer and the Al-O layers shown in Fig. 2(b).

2. $(1\bar{1}02)$ surfaces

Shown in Fig. 3 are top and side views of the sapphire $(1\bar{1}02)$ surface with an O-layer termination. Similar to the (0001) surfaces, the sapphire single crystal may be cleaved parallel to the $(1\bar{1}02)$ plane at three different locations labeled *A*, *B*, and *C* in Fig. 3(b), resulting in five $(1\bar{1}02)$ surfaces with different terminations.

Due to the rectangular shape of the two-dimensional unit mesh of the unreconstructed $(1\bar{1}02)$ surfaces, the cluster atoms were included within a box, which is 4.7 Å wide and 5.0 Å long, for all five surfaces with different

terminations. It was found that the box of 12-Å depth, which includes all the layers shown in Fig. 3(b), is large enough for all five surfaces. Thus, we have five clusters of sizes of 121, 112, 106, 99, and 92 atoms.

B. Formalism

The self-consistent local-density discrete variational method has been used to study the energetics and electronic structure of free molecules and clusters²¹⁻²³ for about two decades. Its extension into the studies of infinite (bulk) systems has proceeded over the past several

years.¹²⁻¹⁹ A complete discussion of the formalism has been presented in the previous works cited above. Therefore, only a brief review will be given here. The ground-state electronic structure of clusters were obtained using the self-consistent discrete variational method. At the beginning of the self-consistent iteration, charge densities for appropriate cations and anions are summed to form the total charge density for the infinite crystal. Coulomb, exchange, and correlation potentials are evaluated as would be required for an ordinary band-structure calculation. A simple pseudopotential is added to atomic sites of the host to represent the Pauli principle exclusion of cluster electrons from the host core region. Here the host is everything not explicitly contained in the variational cluster. Cluster wave functions and energies are

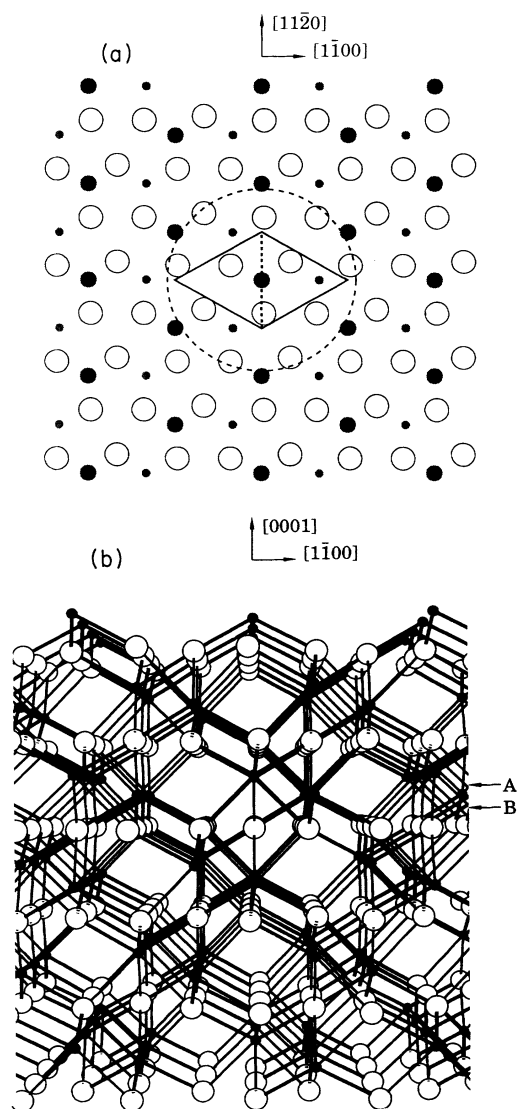


FIG. 2. Sapphirе (0001) surface: (a) top view of one surface building block made up of three atomic layers of Al-O-Al. The open circles label O atoms. The large and small filled circles label Al atoms on the top and the bottom layers. The unit mesh area is enclosed by the solid lines. The dashed circle is the lateral boundary of the cluster. (b) Side view along the $[11\bar{2}0]$ direction. The two arrows labeled A and B indicate the two different (0001) cleaving planes. Same conventions as Fig. 1.

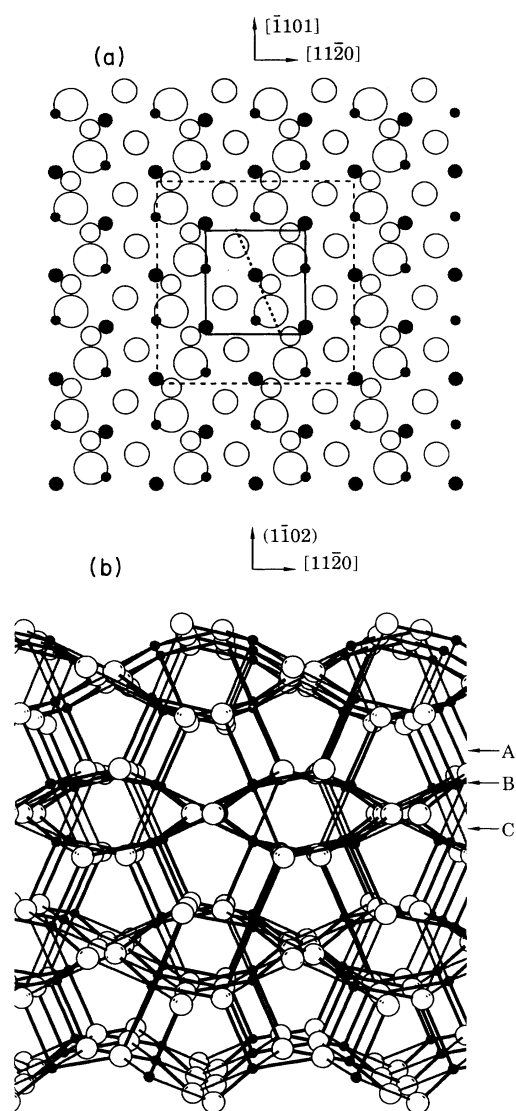


FIG. 3. Sapphirе $(1\bar{1}02)$ surface: (a) top view of one surface building block made up of five atomic layers of O-Al-O-Al-O. The deeper the atom below the top layer, the smaller the radius. Same conventions as Fig. 2. (b) side view along the $[\bar{1}101]$ direction. The three arrows labeled A, B, and C indicate the three different $(1\bar{1}02)$ cleaving planes.

next found by the variational solution of the Schrödinger equation, using a basis set constructed from numerical atomiclike wave functions. The cluster eigenstates are populated according to the Fermi-Dirac statistics to obtain the charge density. The cluster charge density is decomposed according to a scheme similar to the Mulliken population analysis to determine the effective atomic configurations which are then spherically averaged. The iteration loop is closed by summing *seed atom* charge densities to produce new clusters and crystal densities and the iteration is continued until the orbital populations are converged to $< 10^{-3}e$ in the present calculations. This procedure is called the self-consistent-charge approximation to the potential. The embedding potential for the ionic host lattice is obtained by the Ewald summation of long-range Coulomb terms, and direct summation over 200–500 nearby atoms of residual Coulomb potentials and charge densities obtained by self-consistent iterations.

The total energy is calculated in the spin-restricted local-density approximation as²⁴

$$E_i(\rho) = \sum_i \epsilon_i n_i + \int \rho \left(-\frac{1}{2} V_e - V_{xc} + E_{xc} \right) d^3r + \frac{1}{2} \sum'_{\mu, \nu} \frac{Z_\mu Z_\nu}{R_{\mu\nu}}, \quad (1)$$

where i labels single-particle functions with eigenvalue ϵ_i and occupation n_i , ρ is total charge density, V_e is the Coulomb potential due to the electrons, V_{xc} is the exchange-correlation potential, and E_{xc} is the corresponding energy density per electron. The above total energy can be expressed in terms of the energy density as

$$E_i(\rho) = \int e(\mathbf{r}) d^3r + \frac{1}{2} \sum'_{\mu, \nu} \frac{Z_\mu Z_\nu}{R_{\mu\nu}} \quad (2)$$

by rewriting the first term in Eq. (1) as

$$\sum_i \epsilon_i n_i = \int \left(\sum_i \epsilon_i n_i |\Psi_i|^2 \right) d^3r, \quad (3)$$

where Ψ_i is the normalized wave function. The essential assumption of our embedded-cluster method is that the energy density of a crystal over a *finite* volume (e.g., unit cell) can be well approximated by using the eigenvalues and wave functions of the embedded clusters of *finite* sizes. Previous calculations on transition-metal monoxides^{15,16} and the present work on sapphire supported this assumption. This provides us with an effi-

cient way to calculate the various total energies associated with *finite* volumes such as the cohesive energy and the cleavage energy. The total energies calculated in this fashion are of order of 10^5 eV/atom, and it is very difficult and expensive to obtain enough precision for direct comparison of energy difference. However, it is possible to extract a much more precise binding energy with respect to some reference system energy over the same volume with the same sampling grid with the atoms in the same position but now assumed to be noninteracting. In this way, cohesive energy values are obtained to better than 0.01 eV/atom.

The formalism for semi-infinite surfaces is the same as that for infinite bulk material except for those steps given in the following.

1. Surface Coulomb potential

To overcome the slow convergence of bulk lattice sums of the Coulomb potential for ionic crystals, one generally uses the efficient summation scheme of Ewald^{25,26} by introducing a Gaussian charge density associated with site ν as

$$\rho_\nu(\mathbf{r}) = \frac{Q_\nu}{(\sqrt{\pi}a)^3} e^{-r^2/a^2}, \quad (4)$$

where Q_ν is the charge of site ν and a is the width parameter to be chosen later to achieve fast convergence. The corresponding Coulomb potential is

$$U_\nu^G(\mathbf{r}) = \frac{Q_\nu}{r} \operatorname{erf} \frac{r}{a}, \quad \lim_{r \rightarrow \infty} U_\nu^G = \frac{Q_\nu}{r}, \quad (5)$$

where $\operatorname{erf}(r)$ is the error function.

The total Coulomb potential from these Gaussian charges can be evaluated by summation in k space for an infinite bulk crystal under the conditions of periodicity and charge neutrality of the unit cell. However, evaluations of Coulomb potentials for a truncated bulk crystal with a boundary surface is more complex. If one takes the surface normal as the z axis, one is left with (x, y) periodicity to exploit, and a layer-by-layer summation scheme suggests itself naturally. We chose to implement a form similar to that presented by Parry,²⁷ where three-dimensional Gaussians given in Eq. (4) are placed on ion sites.

By two-dimensional Fourier transformation and elementary manipulations, the Coulomb potentials for the two-dimensional layers of Gaussian charge given in Eq. (4) can be placed in the rapidly convergent form

$$V^G(\mathbf{r}) = \frac{\pi}{A} \sum_k' \sum_\nu \frac{Q_\nu}{k} e^{i\mathbf{k} \cdot \mathbf{p}_\nu} \left[e^{kz_\nu} \operatorname{erfc} \left(\frac{ka}{2} + \frac{z_\nu}{a} \right) + e^{-kz_\nu} \operatorname{erfc} \left(\frac{ka}{2} - \frac{z_\nu}{a} \right) \right] + V_0^G, \quad (6)$$

where A is the area of the surface unit mesh, \mathbf{p}_ν and z_ν are the projection of $\mathbf{r} - \mathbf{R}_\nu$ parallel and perpendicular to the surface plane, and $\text{erfc}(x)$ the complementary error function. Here the ν summation is over atoms on all different layers and whose \mathbf{p}_ν is within the surface unit mesh, \mathbf{R}_ν is the position of nuclei of atomic site ν , and the width a can be chosen for rapid convergence both of the real- and of the k -space summations. The first term of the equation above gives the k summation with $k \neq 0$ and the second term V_0^G gives the $k = 0$ contribution described below. The asymptotic form of $V^G(\mathbf{r})$ when $z \rightarrow +\infty$ is given by

$$V^G(\mathbf{r}) = \frac{2\pi}{A} \sum_k' \sum_\nu \frac{Q_\nu}{k} e^{i\mathbf{k}\cdot\mathbf{p}_\nu - kz_\nu}, \quad (7)$$

which allows the summation over an infinite number of identical layers far below the surface by using the equation $(1-z)^{-1} = 1+z+z^2+z^3+\dots$. This asymptotic result is useful for calculating potential far from a surface,²⁸ or for rapid calculation of contributions of layers distant from the field point \mathbf{r} .

As pointed out by Parry, the $k = 0$ term V_0^G in the two-dimensional series does not have a zero value, as is found in three dimensions. Moreover, it plays an important part in determining the z dependence of the asymptotic potential for a crystal cleaved to produce a polar surface. Such cases occur routinely when treating complex oxides. Setting the zero of potential to be the vacuum level, i.e., $\lim_{z \rightarrow +\infty} V = 0$, we have

$$V_0^G(\mathbf{r}) = \frac{2\pi a}{A} \sum_\nu Q_\nu \left(\frac{-1}{\sqrt{\pi}} e^{-(z_\nu/a)^2} + \frac{z_\nu}{a} \text{erfc} \frac{z_\nu}{a} \right). \quad (8)$$

Finally, the surface Coulomb potential is given as

$$V(\mathbf{r}) = \sum_\nu [U_\nu^{\text{Coul}}(\mathbf{r}) - U_\nu^G(\mathbf{r})] + V^G(\mathbf{r}), \quad (9)$$

where U_ν^{Coul} is the Coulomb potential of atomic site ν obtained from the real charge density, U_ν^G is defined in Eq. (5), and ν summation is over the semi-infinite surface lattice.

2. Surface charge density

In the embedded-cluster method, the total charge density of cluster atoms is obtained as

$$\rho_{\text{clust}}(\mathbf{r}) = \sum_{i=1}^{\text{occ}} n_i |\Psi_i|^2, \quad (10)$$

where Ψ_i is the wave function and n_i is the electron occupation number of the i th cluster orbital. The detailed procedures for determining the occupation numbers n_i for the surface calculations are similar to those described for bulk sapphire.¹⁹

In bulk crystals with inversion symmetry, like sapphire, one can always find a unit cell or a cluster containing several unit cells of the infinite crystal lattice which has *neutral charge* and *zero dipole moment*. Furthermore, for such a crystal one can always find a block of atomic layers, with *neutral charge* and *zero dipole moment*, par-

allel to a given crystallographic axis and centered at the site of inversion symmetry. For example, layers Al-O-Al and layers O-Al-O-Al-O are the smallest such blocks for sapphire (0001) and (1 $\bar{1}$ 02) orientations, respectively. However, for semi-infinite surfaces, the three-dimensional unit cell no longer exists and the constraint of charge neutrality of the bulk unit cell needs to be modified. Thus, for surface calculations we need to replace the charge neutrality of the unit cell by the charge neutrality of surface layers of a certain thickness. The construction of *surface neutral units* can be carried out by selecting a number of neutral bulk blocks plus the number of layers required to terminate the desired surface. Such *surface neutral units* guarantee that the macroscopic electric field $\mathbf{E} = -\nabla V(\mathbf{r})$ vanishes at large distance, $\lim_{z \rightarrow \pm\infty} \mathbf{E} = 0$. For example, the *surface neutral units* are O-Al-(Al-O-Al) $_n$, Al-(Al-O-Al) $_n$, and (Al-O-Al) $_n$ for the three different (0001) sapphire surfaces, where the minimum n is determined by the procedure given below.

Since atoms are bulklike far below the surface, we have frozen the charge densities of atoms below the *surface neutral units* to equal those obtained from bulk calculations. Charge densities of atoms inside the *surface neutral units* are determined self-consistently. We determine the extent of the surface effect by successively increasing the depth of the cluster, i.e., increasing the number n of blocks (Al-O-Al) into the cluster self-consistent calculation, until their self-consistently determined charges converge to the values obtained from the bulk calculation. The minimum n was found to be equal to 3 for (0001) and (1 $\bar{1}$ 02) surfaces.

III. RESULTS AND DISCUSSION

A. Cleavage energy and surface atomic termination

The total energy $E(\Omega)$ over a given volume Ω is calculated using a procedure described in the preceding section. For surface calculations, the base of the volume Ω was chosen to be the surface unit mesh, and its height was chosen from the bottom of the third block below the surface, where charge and energy have already converged to the bulk value, up to an infinite distance above the surface. The cleavage energy E_c is calculated as $E_c = E(\Omega_1) + E(\Omega_2) - E(\text{bulk})$, where Ω_1 and Ω_2 are the volumes described above for the two free surfaces resulting from cleaving. $E(\text{bulk})$ is the total energy calculated over the volume of several unit cells which contain the same number of nuclei and electrons as in the volume $\Omega_1 + \Omega_2$.

For the (0001) surfaces, we found that cleaving at plane A shown in Fig. 2(b), which produced two symmetry-equivalent surfaces terminated with an Al layer, has a cleavage energy of 9 eV per unit mesh area (19.64 \AA^2) or 7.4 J/m². The cleavage energy is 17 eV per unit mesh area for cleaving at plane B , which produced two surfaces with different terminations. Therefore, based on the energetic consideration the (0001) surface cleaved from the sapphire single crystal will be terminated with an Al top layer.

For the ($1\bar{1}02$) surfaces, we found that cleaving at plane *A*, which produced two symmetry-equivalent surfaces terminated with an O layer shown in Fig. 3(b), has a cleavage energy of 9 eV per unit mesh area (24.42 \AA^2) or 5.9 J/m^2 . The cleavage energies are 22 and 17 eV for cleaving at the other two planes *B* and *C* shown in Fig. 3(b), respectively. Therefore, the ($1\bar{1}02$) surface is terminated with an O layer.

The cleavage energies given above were calculated while the nuclei are fixed at their bulk positions. We did not allow for local relaxation and reconstruction of the surface. This form of rearrangement can affect the calculated cleavage energies. However, recent energetics calculations on the relaxation of the (0001) surface showed that the relaxation energy is less than 1 eV per unit mesh area.²⁹ In view of the ~ 8 -eV advantage in the cleavage energy per unit mesh area, it is unlikely that the surface relaxation can reverse the trends given above. Furthermore, we have performed calculations on bulk sapphire and a (0001) surface using the von Barth and Hedin exchange and correlation potential³⁰ with and without the Langreth and Mehl (LM) nonlocal corrections.^{31,32} We found that using these different potentials rigidly pulls down the valence band by ~ 1 eV for both the bulk and surfaces and affects the cleavage energy by less than 1 eV per unit mesh area.

Fracture surface energies, which are half of the cleavage energies, of several crystallographic planes of sapphire have been measured by several investigators using different experimental techniques. The reported energy values depend on the crystallographic plane of fracture, the test temperature, sample conditions, and experimental techniques. Congleton *et al.* reported a fracture surface energy of 24 J/m^2 for the ($1\bar{1}02$) plane fractured at $-196 \text{ }^\circ\text{C}$ using a center-notched-plate tension specimen.³³ Wiederhorn reported a fracture surface energy of 6.0 J/m^2 for the same surface at $25 \text{ }^\circ\text{C}$ obtained by a double-cantilever-cleavage measurement.³⁴ Wiederhorn's reported value was derived from averaging all the measured values of 20 samples. Kingery obtained a fracture surface energy of $\sim 1 \text{ J/m}^2$ using equilibrium interfacial angle measurements at $1850 \text{ }^\circ\text{C}$.³⁵ The fracture surface energy thus obtained only represents an average value for all the crystallographic planes of sapphire. Wiederhorn was not able to obtain a fracture surface energy for the (0001) plane because the crack propagated on several lower-energy fracture surfaces instead of the (0001) plane in the fracture experiment. He gave an estimated value of $\sim 40 \text{ J/m}^2$ for the fracture surface energy of (0001).

The calculated fracture surface energy of 3.0 J/m^2 for the ($1\bar{1}02$) plane is lower than the experimental values reported by Wiederhorn and Congleton *et al.* The average fracture surface energy of 6.0 J/m^2 for the ($1\bar{1}02$) plane obtained by Wiederhorn seems to be more reliable because this average value and the standard deviation of 0.6 J/m^2 were derived from 21 determinations of annealed and as-received single-crystal specimens. Our calculated value is about half of the experimental value of Wiederhorn. The calculated fracture surface energy of 3.7 J/m^2 for the (0001) plane is much lower than the

estimated value of Wiederhorn. The fact that the calculated fracture surface energy for the (0001) plane is higher than that of the ($1\bar{1}02$) seems to follow the experimental trend.

From the energetic calculations for (0001) and ($1\bar{1}02$) sapphire surfaces with all possible terminations, we found that cleaving at the block boundary costs the least cleavage energy compared with those within the block. This leads us to call such a repeating unit the *surface building block*. For the (0001) surface, the *surface building block* consists of (Al-O-Al) atomic layers and for ($1\bar{1}02$) surface, it consists of (O-Al-O-Al-O) layers. The concept of the *surface building block* can serve as a useful guide to determine the surface atomic termination of complex surfaces.

B. Surface density of states

We optimized the basis functions using the same procedures described for bulk sapphire.¹⁹ To have sufficient variational freedom of the basis due to the introduction of surfaces, we add the $3d$ orbitals into the minimum basis of $1s2s2p3s3p$ for all the Al atoms.

1. Analysis of the low-energy (0001) surface

Shown in Fig. 4(a) are Al and O partial density of states (PDOS) of the top three surface building blocks for the (0001) surfaces with low cleavage energy, which is terminated with an Al layer. The PDOS shown in Fig. 4 are normalized to one molecular formula unit of $\alpha\text{-Al}_2\text{O}_3$ per unit mesh area and convoluted by a Lorentzian function of 0.5 eV full width at half maximum height. The zero of energy for all curves is the vacuum level, which is defined as the potential value far above the surface.

The shape of Al and O PDOS of the third surface building block shown at the top of Fig. 4(a) has already converged to those bulk PODS obtained from the bulk calculations.¹⁹ The 11-eV band gap from -3.5 to 7.5 eV between the Al and O PDOS also agrees with the value from the bulk calculations, and serves as a reference for the two empty Al surface states at -0.5 and 5.5 eV shown in Fig. 4(a). Detailed orbital analysis reveals that the surface state at -0.5 eV, belonging to the *a* irreducible representation, is mainly made up of the $3s$ and $3p_z$ atomic orbitals of the top Al layer and the $2p_z$ orbital of the O layer underneath at -1.59 a.u.; the state at 5.5 eV, belonging to the *e* irreducible representation, is mainly made up of the $3p_{xy}$ and $3d$ atomic orbitals of the top Al layer. For the topmost building block, the lower valence band (LVB) is 1 eV narrower than the two blocks below, while the upper valence band (UVB) is 1 eV wider. The energy averages of the valence bands of the topmost building block and second blocks are shifted upward and downward by 1 eV relative to those of the third block, respectively. These energy shifts arise from the nonzero dipole moments of the *surface building blocks* near the surface.

Ciraci and Batra¹¹ have investigated electronic structure of a sapphire (0001) surface using a semiempirical

method. They simulated the surface by a slab having the thickness of the hexagonal cell and a threefold rotation axis along z . The slab unit cell contains 12 Al and 18 O atoms in accord with the bulk stoichiometry, as in Fig. 1. Al atoms form the topmost surface layers on both sides of the slab in contrast to the present calculation. They found two surface-state bands located in the gap. A flat band lying at ~ 3 eV above the valence-band maximum (VBM) is due to the $s + p_z$ dangling bonds of the surface Al atoms with a small O orbital contribution from the second layer. This band is thus identical to the presently calculated surface states at -0.5 eV (~ 3 eV

above the VBM). They also found a band of surface states at the edge of the conduction band which are produced mainly by Al $3p_{x,y}$ orbitals. This band corresponds to the gap states at 5.5 eV in the present calculation. It is not surprising that the two calculated surface electronic structures have such good agreement since both calculations started with almost identical atomic structure to the sapphire (0001) surface. Ciraci and Batra used a slab of Al_2O_3 with two Al surfaces, in contrast to the present calculation with a semi-infinite crystal. In fact, the slab calculation contains exactly six (Al-O-Al) *building blocks*, which according to our results is the minimum needed to achieve bulk structure at the center.

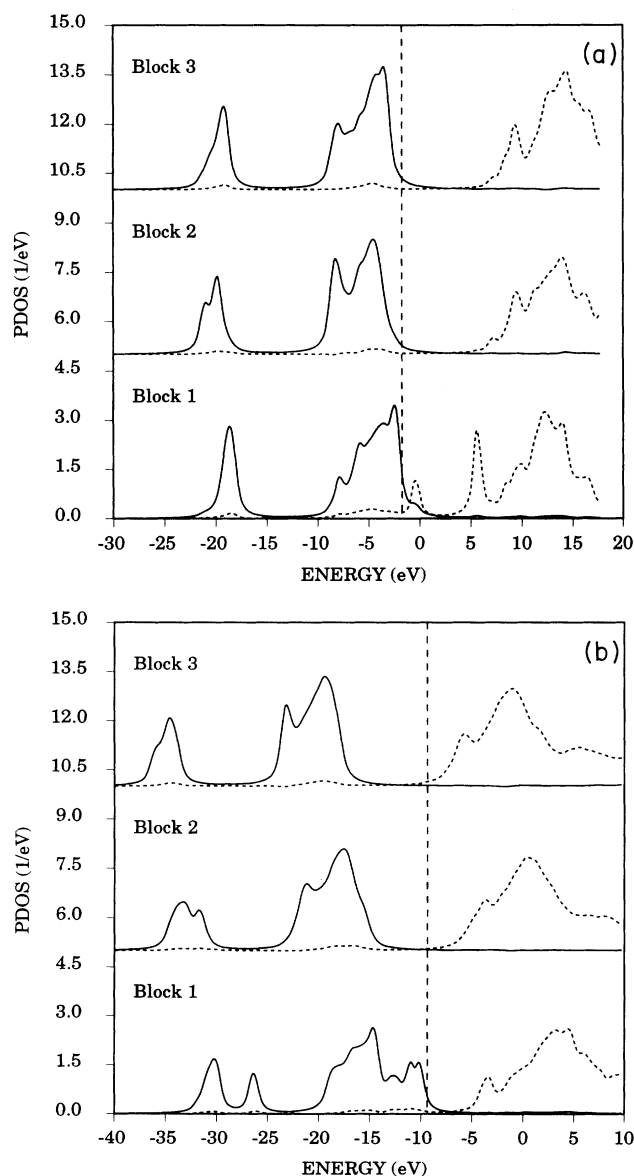


FIG. 4. Al (dashed curve) and O (solid curve) partial density of states of the top three surface building blocks for sapphire (a) (0001) surface and (b) ($1\bar{1}02$) surface. Curves are shifted upwards for a clear view. The vertical dashed line separates the occupied states in the left-hand side from the unoccupied states in the right-hand side. The zero of energy scale for all curves is the vacuum level.

2. Analysis of the low-energy ($1\bar{1}02$) surface

Shown in Fig. 4(b) are Al and O partial density of states (PDOS) of the top three surface building blocks for the ($1\bar{1}02$) surfaces with low cleavage energy, which is terminated with an O layer. Similar to the (0001) surface, the Al and O PDOS of the third surface building block shown at the top of Fig. 4(b) have already converged to the bulk values and define the 11-eV band gap from -18 to -7 eV. From Fig. 4(b), we see that the extra features due to the $2s2p$ states of the top O layers in the topmost and second building blocks are shifted 5 and 2 eV relative to the main features. The peaks at -27 eV and around -10 eV in the O PDOS of the topmost block are due to the occupied $2s$ and $2p$ valence states of the top surface O layer, respectively.

The valence- and conduction-band density of states of the sapphire ($1\bar{1}02$) surface have been investigated by Gignac, Williams, and Kowalczyk using x-ray photoelectron (XPS) and electron-energy-loss (EELS) spectroscopies.¹⁰ They found an energy-loss feature at 4.7-eV loss energy. The electron kinetic-energy-dependent behavior of this loss feature is what one would expect if either the initial or final state of the interband transition was a surface state. They interpreted this interband transition as the result of a transition of electrons from an initial state in the O valence band to an empty Al surface state located at 4.0 eV below the conduction-band minimum (CBM). They compared the experimental results with the theoretical density of states of the (0001) surface calculated by Ciraci and Batra. As discussed in the preceding section, the character of the surface states in the (0001) surface is very much different from the surface states in the ($1\bar{1}02$) surface. The surface states at ~ 3 eV above the VBM in the (0001) surface is an empty state produced by the $s + p_z$ dangling bonds of the surface Al atoms. On the other hand, the gap states at ~ 4.0 eV below the CBM on the ($1\bar{1}02$) surface are occupied $2p$ states produced by the top O surface layer. Based on the present result, we will assign the 4.7-eV loss feature to the interband transition of electrons from the initial occupied O surface state to the empty Al conduction-band final state.

To compare further with the experiment, we plot in Fig. 5 the raw experimental XPS data reproduced from Fig. 1(a) of Ref. 10 and the calculated XPS cross sec-

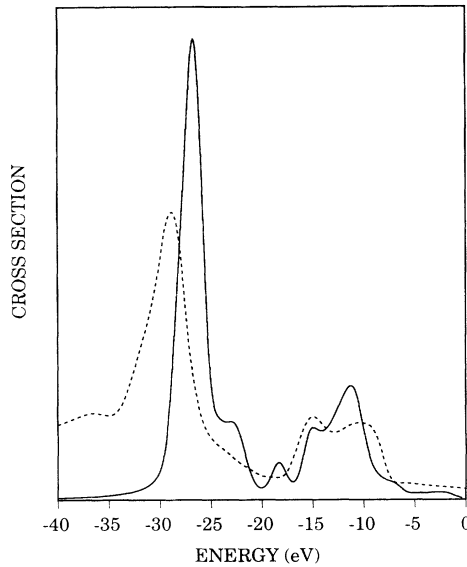


FIG. 5. The calculated (solid curve) and the experimental XPS cross section (dotted curve). The experimental data are reproduced from Fig. 1(a) of Ref. 10.

tion for the top eight surface building blocks with a total depth of 28 Å simulating the photoelectron escape depth. The XPS cross section is approximately calculated as the product of the occupied O 2*s* and 2*p* PDOS and the corresponding O subshell photoionization cross sections from Scofield.³⁶ The calculated cross section is convoluted by a Gaussian function with 1 eV full width at half maximum height to facilitate the comparison with experiment. From Fig. 5, we see that the calculated locations of the two main peaks of UVB agree well with the experiment, while the calculated main peak of LVB is located ~2 eV higher than the experimental one. This may be due to the neglect of relaxations of the O 2*s* corelike electrons in our present ground-state calculations.

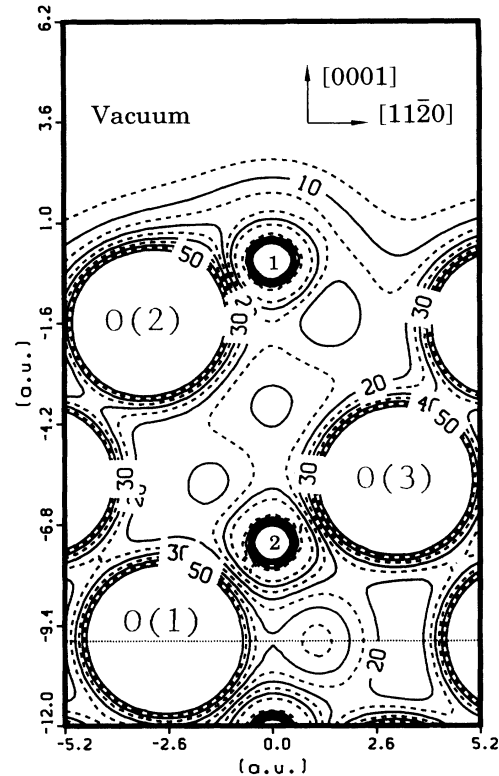


FIG. 6. The valence charge-density contour diagrams on the cross-section ($1\bar{1}00$) plane containing the dotted line shown in Fig. 2(a) for the (0001) surface. The atom labels are the same as those in Fig. 1. The minimum and maximum contours are 0.005 and $0.050e/a_0^3$, and the contour interval is $0.005e/a_0^3$.

C. Surface charge and dipole density

We list in Tables I and II the layer-by-layer Mulliken orbital populations, charge and surface dipole density of

TABLE I. The Mulliken orbital populations, charges, and surface dipole density for the top three surface building blocks of the (0001) surface and for bulk sapphire. The dipole densities are relative to the center of individual blocks.

Layer height (a.u.)	Atom type	Orbital population (<i>e</i>)	Charge (<i>e</i>)	Dipole density 10^{-2} (<i>e/a</i> ₀)
0.00	Al	$3s^{0.20} 3p^{0.15} 3d^{0.04}$	2.61	
-1.59	O	$2s^{2.00} 2p^{5.83}$	-1.83	
-3.17	Al	$3s^{0.01} 3p^{0.06} 3d^{0.08}$	2.85	
			-0.04	-0.55
-4.09	Al	$3s^{0.01} 3p^{0.03} 3d^{0.06}$	2.90	
-5.68	O	$2s^{2.00} 2p^{5.90}$	-1.90	
-7.26	Al	$3s^{0.01} 3p^{0.04} 3d^{0.07}$	2.89	
			0.09	0.02
-8.18	Al	$3s^{0.01} 3p^{0.04} 3d^{0.07}$	2.89	
-9.77	O	$2s^{2.00} 2p^{5.94}$	-1.94	
-11.35	Al	$3s^{0.01} 3p^{0.04} 3d^{0.07}$	2.89	
			-0.05	0.00
Bulk	Al	$3s^{0.01} 3p^{0.04} 3d^{0.08}$	2.87	0.00
Bulk	O	$2s^{2.00} 2p^{5.91}$	-1.91	0.00

TABLE II. The Mulliken orbital populations, charges, and surface dipole density for the top three surface building blocks of the $(1\bar{1}02)$ surface. Same conventions as Table I.

Layer height (a.u.)	Atom type	Orbital population (e)	Charge (e)	Dipole density 10^{-2} (e/a_0)
0.00	O	$2s^{2.00}2p^{5.91}$	-1.91	
-0.67	Al	$3s^{0.05}3p^{0.08}3d^{0.08}$	2.79	
-2.01	O	$2s^{2.00}2p^{5.85}$	-1.85	
-3.36	Al	$3s^{0.05}3p^{0.08}3d^{0.09}$	2.78	
-4.03	O	$2s^{1.99}2p^{5.86}$	-1.85	
			-0.11	-0.24
-6.58	O	$2s^{2.00}2p^{5.93}$	-1.93	
-7.25	Al	$3s^{0.02}3p^{0.05}3d^{0.09}$	2.84	
-8.59	O	$2s^{2.00}2p^{5.84}$	-1.84	
-9.93	Al	$3s^{0.01}3p^{0.05}3d^{0.08}$	2.86	
-10.60	O	$2s^{2.00}2p^{5.88}$	-1.88	
			0.09	-0.27
-13.16	O	$2s^{2.00}2p^{5.91}$	-1.91	
-13.83	Al	$3s^{0.03}3p^{0.05}3d^{0.08}$	2.85	
-15.17	O	$2s^{2.00}2p^{5.87}$	-1.87	
-16.51	Al	$3s^{0.04}3p^{0.05}3d^{0.08}$	2.84	
-17.18	O	$2s^{2.00}2p^{5.90}$	-1.90	
			0.02	-0.04
Bulk	Al	$3s^{0.01}3p^{0.04}3d^{0.08}$	2.87	0.00
Bulk	O	$2s^{2.00}2p^{5.91}$	-1.91	0.00

the top three surface building blocks for the (0001) and $(1\bar{1}02)$ surface, respectively. The dipole densities listed are relative to the center of individual surface building blocks. The orbital populations obtained from bulk cal-

culations are also listed for comparison. From Tables I and II, we see a considerable redistribution of electrons within the top two building blocks. The third building block below the surface is rather bulklike in terms of its charge distribution and dipole moment.

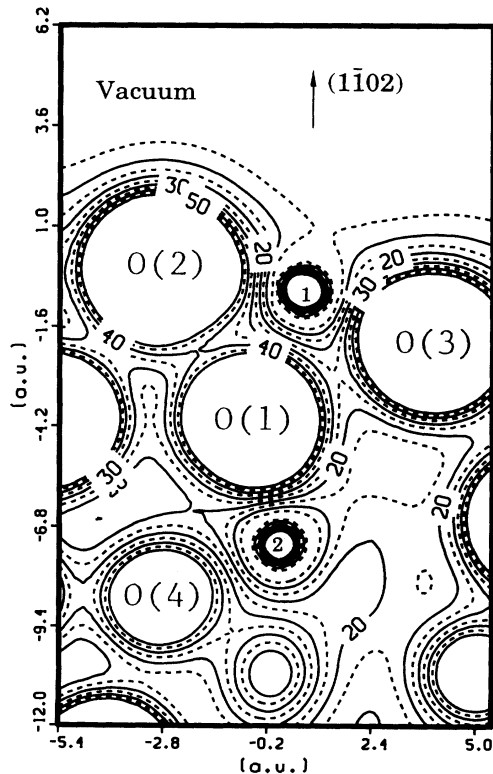


FIG. 7. The valence charge-density contour diagram on the cross-section plane containing the dotted line shown in Fig. 3(a) for the $(1\bar{1}02)$ surface. Same conventions as in Fig. 6.

1. Analysis of the low-energy (0001) surface

In Fig. 6, we have plotted the valence electron density contour diagram of a $(1\bar{1}00)$ cross-section plane indicated by the dotted line in Fig. 2(a) with the core density omitted. The atoms Al(1), Al(2) and O(1) are all on the contour plane, and the two O atoms labeled as O(2), O(3) are ± 0.21 a.u. off the plane. The Al-O bonds between Al(1)-O(2) and Al(2)-O(3) are the short bond (3.51 a.u.), and the Al-O bond between Al(2)-O(1) is the long bond (3.72 a.u.). We see changes in the charge density along the short Al-O bond at the surface Al(1)-O(2) compared to the short Al-O bond below Al(2)-O(3). However, the short Al-O bond Al(2)-O(3) and long Al-O bond Al(2)-O(1) are quite similar and have no charge accumulation along the bonds, indicating essentially ionic bonding. The horizontal line passing through the nucleus of O(1) is the twofold rotational axis of the sapphire crystal. This symmetry is broken due to the creation of the surface. However, the approximate reflection symmetry of the charge density about this horizontal line indicates that the charge density in regions 9.5 a.u. below the surface is already bulklike, in agreement with the analysis of density of states in the preceding section.

2. Analysis of the low-energy $(1\bar{1}02)$ surface

Figure 7 is a contour diagram of the valence electron density on a plane perpendicular to the $(1\bar{1}02)$ plane as

indicated by the dotted line in Fig. 3(a). This plane was chosen to display Al-O bonds to best advantage. Atoms Al(1) and O(2) are on the contour plane, and the atoms Al(2), O(1), O(3), and O(4) are off the plane. The atom Al(1) is bonded with O(1) and O(2) through long Al-O bonds and with O(3) through short Al-O bonds. The Al(2) is bonded with O(1) and O(4) through short and long Al-O bonds, respectively. We can see changes in the charge density along the short Al(1)-O(3) and long Al-O Al(1)-O(2) bonds at the surface compared to the corresponding ones below the surface.

IV. CONCLUSIONS

We have used the first-principles embedded-cluster method to calculate electronic structure and energetics for sapphire (0001) and (1 $\bar{1}$ 02) surfaces. The energetics calculations show that the surface with the lowest cleavage energy is terminated with an Al layer for the (0001) surface, while it is terminated with an O layer

for the (1 $\bar{1}$ 02) surface. The proposed concept of the *surface building block* can serve as a useful guide to determine the surface atomic termination of complex surfaces. Two unoccupied surface bands derived from the top-layer Al atoms are found within the bulk band gap at 2 and 8 eV below the CBM for the (0001) surface. For the (1 $\bar{1}$ 02) surface, the occupied valence states derived from 2p states of the top-layer O atoms are found ~4.5 eV below the CBM, which may explain the 4.7-eV energy-loss feature found experimentally on a sapphire (1 $\bar{1}$ 02) surface.

ACKNOWLEDGMENTS

The work is supported by the U.S. Department of Energy (Division of Materials Science of the Office of Basic Energy Sciences) under Contract No. W-31-109-Eng-38 and by a grant of computer time on Cray computers from the National Energy Research Supercomputer Center and Florida State University. The work of D.E.E. was supported in part by Grant No. DE-FG02-84ER45097.

- ¹E. Dorre, *Alumina: Processing Properties and Applications* (Springer-Verlag, New York, 1984).
- ²J. M. Charig, *Appl. Phys. Lett.* **10**, 139 (1967).
- ³C. C. Chang, *J. Appl. Phys.* **39**, 5570 (1968).
- ⁴T. M. French and G. A. Somorjai, *J. Phys. Chem.* **74**, 2489 (1970).
- ⁵D. W. Susnitzky and C. B. Carter, *J. Am. Ceram. Soc.* **69**, C-217 (1986).
- ⁶S. Baik, D. E. Fowler, J. M. Balkely, and R. Raj, *J. Am. Ceram. Soc.* **68**, 281 (1985).
- ⁷C. C. Chang, in *Proceedings of the Conference on the Structure and Chemistry of Solid Surfaces*, edited by G. A. Somorjai (Wiley, New York, 1969), p. 77.
- ⁸N. Yao, Z. L. Wang, and J. M. Cowley, *Surf. Sci.* **208**, 533 (1989).
- ⁹T. Hsu and Y. Kim, *Surf. Sci.* **243**, L63 (1991).
- ¹⁰W. J. Gignac, R. S. Williams, and S. P. Kowalczyk, *Phys. Rev. B* **32**, 1237 (1985).
- ¹¹S. Ciraci and I. P. Batra, *Phys. Rev. B* **28**, 982 (1983).
- ¹²S.-H. Chou, J. Guo, and D. E. Ellis, *Phys. Rev. B* **34**, 12 (1986).
- ¹³W. Y. Ching, D. E. Ellis, and D. J. Lam, in *Phase Transitions in Condensed Systems: Experiments and Theory*, edited by D. Turnbull, G. S. Cargill, F. Spaepen, and K. N. Tu, MRS Symposia Proceedings No. 82 (Materials Research Society, Pittsburgh, 1987), p. 181.
- ¹⁴S. Xia, C. Guo, L. Lin, and D. E. Ellis, *Phys. Rev. B* **35**, 7671 (1987).
- ¹⁵M. R. Press and D. E. Ellis, *Phys. Rev. B* **35**, 4438 (1987).
- ¹⁶P. K. Khowash and D. E. Ellis, *Phys. Rev. B* **36**, 3394 (1987); **39**, 1908 (1989).
- ¹⁷D. E. Ellis, J. Guo, and D. J. Lam, *J. Am. Ceram. Soc.* **73**, 3231 (1990).
- ¹⁸G. L. Goodman, D. E. Ellis, E. E. Alp, and L. Soderholm, *J. Chem. Phys.* **91**, 2983 (1989).
- ¹⁹J. Guo, D. E. Ellis, and D. J. Lam, *Phys. Rev. B* **45**, 3204 (1992).
- ²⁰R. W. G. Wyckoff, *Crystal Structures II*, 2nd ed. (Wiley, New York, 1964).
- ²¹E. J. Baerends, D. E. Ellis, and P. Ros, *Chem. Phys.* **2**, 41 (1973).
- ²²A. Rosén, D. E. Ellis, H. Adachi, and F. W. Averill, *J. Chem. Phys.* **65**, 3629 (1976).
- ²³D. E. Ellis, J. Guo, and H.-P. Cheng, *J. Phys. Chem.* **92**, 3024 (1988).
- ²⁴B. Delley, D. E. Ellis, A. J. Freeman, E. J. Baerends, and D. Post, *Phys. Rev. B* **27**, 2132 (1983).
- ²⁵P. P. Ewald, *Ann. Phys.* **64**, 253 (1921).
- ²⁶M. P. Tosi, in *Solid State Physics*, edited by H. Ehrenreich, F. Seitz, and D. Turnbull (Academic, New York, 1964), p. 107.
- ²⁷D. E. Parry, *Surf. Sci.* **49**, 433 (1975); **54**, 195 (1976).
- ²⁸R. E. Watson, J. W. Davenport, M. L. Perlman, and T. K. Sham, *Phys. Rev. B* **24**, 1791 (1981).
- ²⁹J. Guo, D. E. Ellis, and D. J. Lam (unpublished).
- ³⁰U. von Barth and L. Hedin, *J. Phys. C* **5**, 1629 (1972).
- ³¹D. C. Langreth and M. J. Mehl, *Phys. Rev. Lett.* **47**, 446 (1981).
- ³²D. C. Langreth and M. J. Mehl, *Phys. Rev. B* **28**, 1809 (1983).
- ³³J. Congleton, H. Hardie, R. N. Perkins, and N. J. Petch, Technical Report ASD-TR-61-628, Part III; Contract AF 33(657)-10697 (1964), pp. 133-174 (unpublished).
- ³⁴S. M. Wiederhorn, *J. Am. Ceram. Soc.* **52**, 485 (1969).
- ³⁵W. D. Kingery, *J. Am. Ceram. Soc.* **37**, 42 (1954).
- ³⁶J. H. Scofield, *J. Electron. Spectrosc.* **8**, 129 (1976).

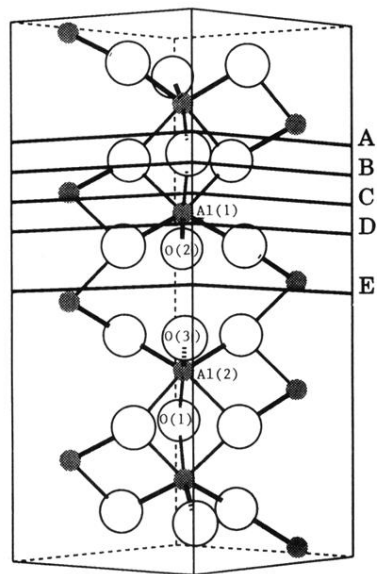


FIG. 1. A perspective view of the hexagonal unit cell of sapphire. The filled circles label Al atoms, and open circles O atoms. The dark thick lines label the short Al-O bonds (1.86 Å), the light thin lines the long Al-O bonds (1.97 Å).

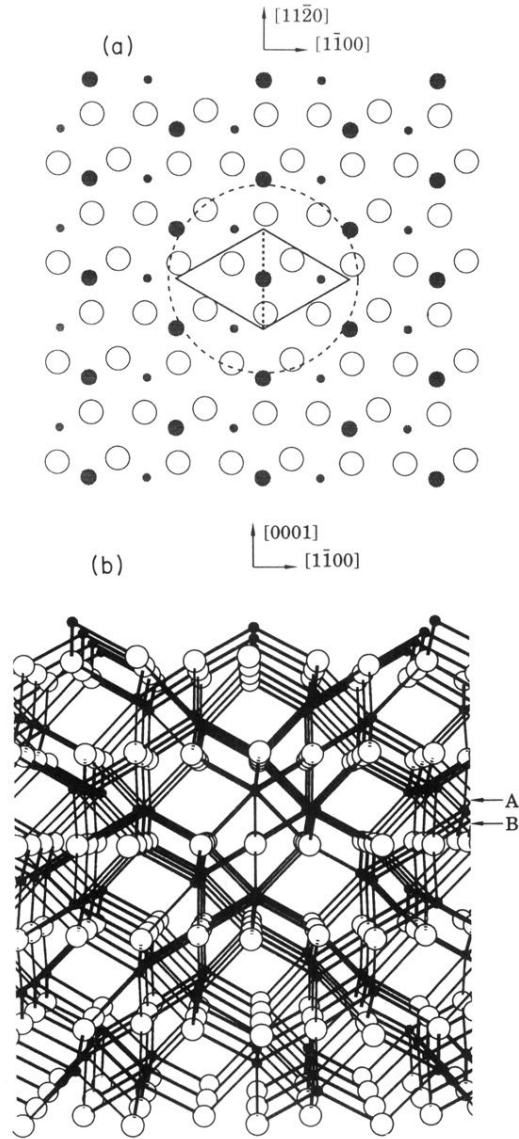


FIG. 2. Sapphire (0001) surface: (a) top view of one surface building block made up of three atomic layers of Al-O-Al. The open circles label O atoms. The large and small filled circles label Al atoms on the top and the bottom layers. The unit mesh area is enclosed by the solid lines. The dashed circle is the lateral boundary of the cluster. (b) Side view along the $[11\bar{2}0]$ direction. The two arrows labeled *A* and *B* indicate the two different (0001) cleaving planes. Same conventions as Fig. 1.

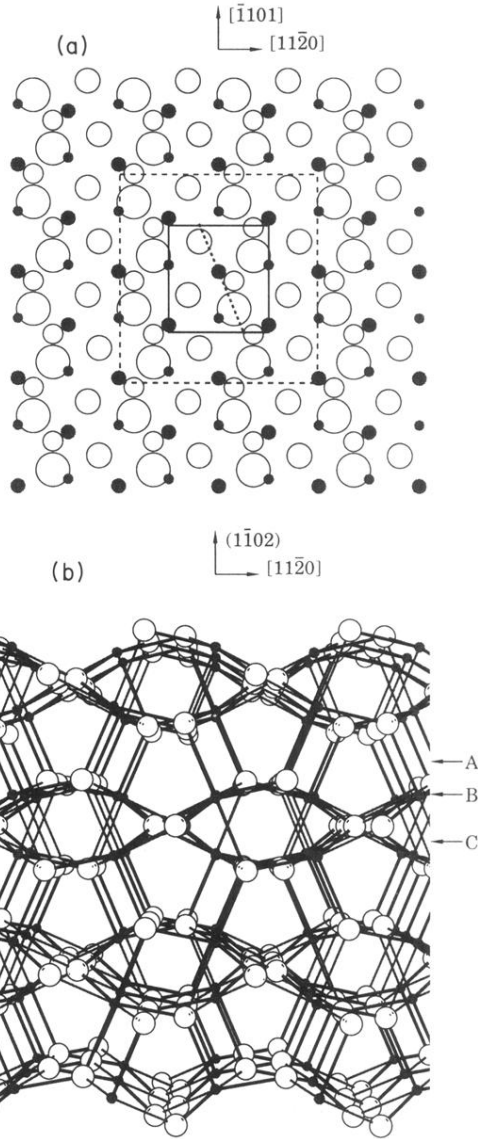


FIG. 3. Sapphire $(\bar{1}\bar{1}02)$ surface: (a) top view of one surface building block made up of five atomic layers of O-Al-O-Al-O. The deeper the atom below the top layer, the smaller the radius. Same conventions as Fig. 2. (b) side view along the $[\bar{1}\bar{1}01]$ direction. The three arrows labeled *A*, *B*, and *C* indicate the three different $(\bar{1}\bar{1}02)$ cleaving planes.